nature neuroscience

Tbr1 haploinsufficiency impairs amygdalar axonal projections and results in cognitive abnormality

Tzyy-Nan Huang[1,4], Hsiu-Chun Chuang[1,2,4], Wen-Hsi Chou[1], Chiung-Ya Chen[1], Hsiao-Fang Wang[1], Shen-Ju Chou[3] & Yi-Ping Hsueh[1,2]

The neuron-specific transcription factor T-box brain 1 (TBR1) regulates brain development. Disruptive mutations in the *TBR1* gene have been repeatedly identified in patients with autism spectrum disorders (ASDs). Here, we show that *Tbr1* haploinsufficiency results in defective axonal projections of amygdalar neurons and the impairment of social interaction, ultrasonic vocalization, associative memory and cognitive flexibility in mice. Loss of a copy of the *Tbr1* gene altered the expression of *Ntng1*, *Cntn2* and *Cdh8* and reduced both inter- and intra-amygdalar connections. These developmental defects likely impair neuronal activation upon behavioral stimulation, which is indicated by fewer c-FOS–positive neurons and lack of GRIN2B induction in *Tbr1*$^{+/-}$ amygdalae. We also show that upregulation of amygdalar neuronal activity by local infusion of a partial NMDA receptor agonist, D-cycloserine, ameliorates the behavioral defects of *Tbr1*$^{+/-}$ mice. Our study suggests that TBR1 is important in the regulation of amygdalar axonal connections and cognition.

Defects in neural development alter brain circuit formations and may result in lethality, mental retardation or psychiatric disorders. Transcription factors have been shown to make key contributions to brain development. TBR1, a T-box transcription factor, is specifically expressed in the cerebral cortex, hippocampus, amygdala and olfactory bulb[1,2]. *Tbr1*$^{-/-}$ mice have been characterized by neonatal lethality, severe defects in the axonal projections of the cerebral cortex and impairment of neuronal migration of the cerebral cortex and amygdala[2,3], indicating the important role of Tbr1 in forebrain development. Recently, whole-exome sequencing has further indicated that *TBR1* is one of six hot targets with recurrent *de novo* mutations in patients with ASDs[4–10]. ASDs are characterized by reduced social interaction, lack of communication, defective cognitive flexibility and intellectual impairment. In patients carrying a mutation in the *TBR1* gene, only one of the alleles was disrupted[6,7,10], suggesting that loss of a *TBR1* allele likely influences brain function. In this report, we investigated whether *Tbr1* haploinsufficiency results in anatomic defects and cognitive impairment.

RESULTS

Amygdalar axonal projections are defective in *Tbr1*$^{+/-}$ mice

We first compared the brain anatomy of wild-type, *Tbr1*$^{+/-}$ and *Tbr1*$^{-/-}$ mice. As found in a previous study[3], neuronal migration of the cerebral cortex was severely impaired in *Tbr1*$^{-/-}$ brains (**Supplementary Fig. 1a–c**). In contrast, loss of one allele of *Tbr1* did not obviously influence the lamination of the cerebral cortex (**Supplementary Fig. 1a–c**). MRI (magnetic resonance imaging) and histological studies also did not detect defects in the cerebral cortex of *Tbr1*$^{+/-}$ mice when size, lamination and axonal projections were compared with those of wild-type littermates (**Supplementary Figs. 1d–f**, **2** and **3**). However, we noticed that the posterior part of the anterior commissure was missing in all of the analyzed *Tbr1*$^{+/-}$ mice (**Fig. 1a**,**b** and **Supplementary Fig. 1d**,**g**), suggesting that the posterior part of the anterior commissure is the anatomic structure most sensitive to *Tbr1* haploinsufficiency.

Because the posterior part of the anterior commissure links the two amygdalae in the two hemispheres, the lack of this structure suggests that the inter-amygdalar connection is impaired in *Tbr1*$^{+/-}$ brains. To examine this possibility, we carried out tracing and retrograde labeling with the lipophilic dye DiI-C_{18}(3) (**Fig. 1c**). Implantation of DiI in the basolateral amygdala labeled the posterior part of the anterior commissure in wild-type littermates, but not in *Tbr1*$^{+/-}$ brains (**Fig. 1d**). When retrograde red beads were implanted into the lateral amygdala, the fluorescent signals of the red beads were clearly detected in the contralateral amygdala in wild-type littermates, but fewer signals were observed in the *Tbr1*$^{+/-}$ amygdala (**Fig. 1e–g**), indicating that the inter-amygdalar connections were greatly diminished in *Tbr1*$^{+/-}$ mice. In addition to the contralateral amygdala, the basolateral amygdala also projects to the ipsilateral central amygdala. We found that implantation of red beads into the central amygdala also revealed defects in the connection between the ipsilateral central amygdala and basolateral amygdala in *Tbr1*$^{+/-}$ mice (**Fig. 1h–j**). It was noted that in wild-type mice, the variability of retrograde labeling was high. Such high variability is likely due to the different injection sites at the central amygdala because the central amygdala receives multiple inputs from various nuclei[11].

TBR1 likely acts cell-autonomously to control amygdalar axonal projections, because, similar to the situation in the cerebral cortex,

[1]Institute of Molecular Biology, Academia Sinica, Taipei, Taiwan. [2]Graduate Institute of Life Sciences, National Defense Medical Center, Taipei, Taiwan. [3]Institute of Cellular and Organismic Biology, Academia Sinica, Taipei, Taiwan. [4]These authors contributed equally to this work. Correspondence should be addressed to Y.-P.H. (yph@gate.sinica.edu.tw).

Received 25 July 2013; accepted 11 December 2013; published online 19 January 2014; doi:10.1038/nn.3626

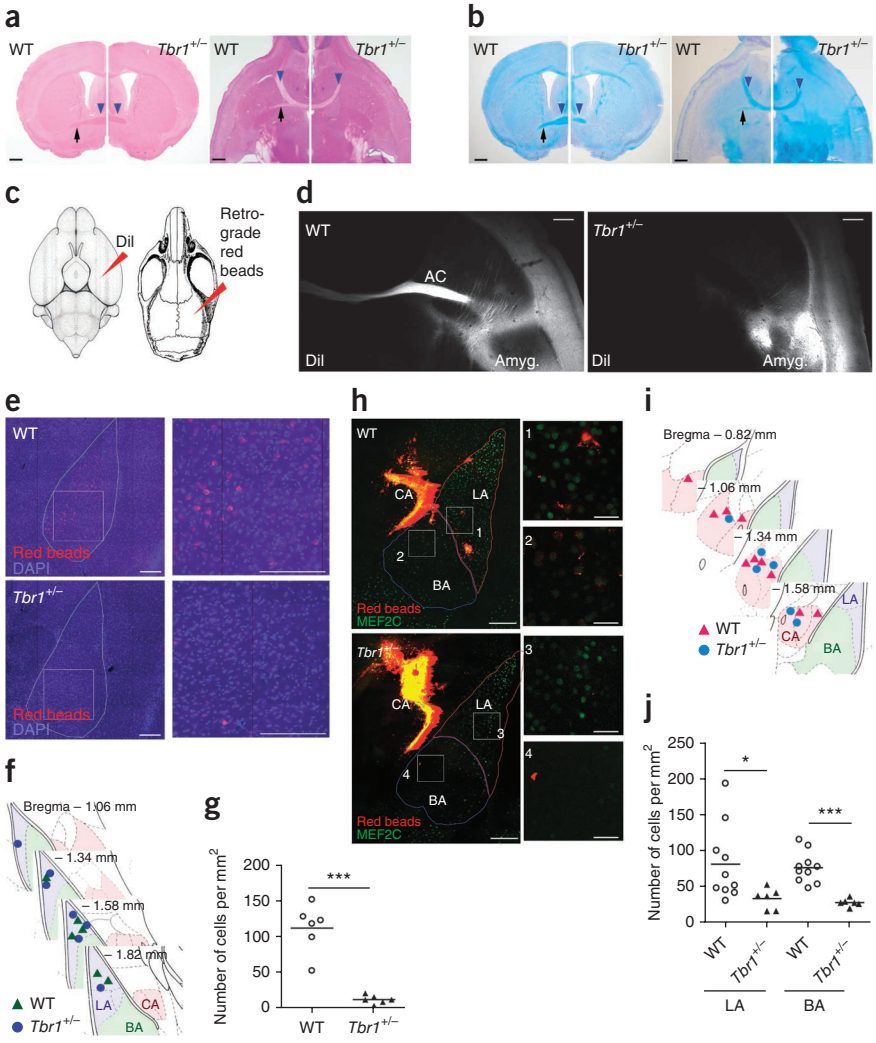

Figure 1 *Tbr1* haploinsufficiency impairs both inter- and intra-amygdalar axonal projections. (**a**,**b**) Hematoxylin and eosin staining (**a**) and Luxol fast blue/cresyl violet staining (**b**) of brain sections. Blue arrowheads point to the anterior part of the anterior commissure (AC); black arrows point to the posterior part of the anterior commissure. (**c**) Diagrams of the mouse brain and skull; red arrowheads indicate the sites of tracer injection. (**d**) Images of the DiI tracing. DiI was implanted into the basolateral amygdala. The tracing failed to detect an axonal pathway from the amygdala (Amyg.) to the anterior commissure in *Tbr1*$^{+/-}$ mice. (**a**,**b**,**d**) Representative images are shown. The same results were found in 18 wild-type and 18 *Tbr1*$^{+/-}$ mice (**a**,**b**) and 5 wild-type and 5 *Tbr1*$^{+/-}$ mice (**d**). (**e**–**j**) Inter-amygdalar (**e**–**g**) and intra-amygdalar (**h**–**j**) retrograde tracing using red beads. LA, lateral amygdala; CA, central amygdala; BA, basal amygdala. The implantation sites are indicated in the lateral amygdala (**f**) and the central amygdala (**i**). The retrograde labeling was monitored in the contralateral side of the basolateral amygdala (**e**) and the ipsilateral lateral amygdala and basal amygdala (**h**). Immunostaining using the MEF2C antibody (green) showed the morphology of the lateral amygdala in **h**. In both **e** and **h**, high magnification images of the insets are shown in the right panels. (**g**,**j**) Quantification of the total number of cells positive for the red beads. Each dot indicates the results obtained from an individual animal. The horizontal lines represent the means. (**g**) $P < 0.001$, $t = 7.158$, d.f. = 10. (**j**) LA $P = 0.048$, $t = 2.159$, d.f. = 14; BA $P < 0.001$, $t = 5.311$, d.f. = 14. Scale bars: 1 mm (**a**,**b**); 400 μm (**d**); 200 μm (**e**); 200 μm (**h**); 50 μm (**h**, insets). $^{*}P < 0.05$; $^{***}P < 0.001$.

TBR1 is expressed in projection neurons labeled by CaMKII in both lateral and basal amygdala (**Supplementary Fig. 4**)[3]. Other than the axonal phenotypes, we did not find further anatomic defects in *Tbr1*$^{+/-}$ amygdalae (**Supplementary Fig. 5**).

Genes downstream of TBR1 control amygdalar axon outgrowth

We then explored how *Tbr1* haploinsufficiency results in axonal defects in the amygdala. Our previous studies indicated that TBR1 regulates *Reln* and *Grin2b* expression[12–15]. In addition to these two genes, we used microarray analysis to identify 90 more genes from embryonic forebrains as downstream targets of TBR1 (**Supplementary Table 1**). We first confirmed changes in the expression of some of the genes in *Tbr1*$^{+/-}$ forebrains (**Fig. 2a–c**). Among these genes, *Ntng1*, *Cdh8* and *Cntn2* were of particular interest because these genes control neurite outgrowth and fasciculation[16–20]. These genes are also expressed in the amygdala (Allen Brain Atlas; http://www.brain-map.org/). To investigate whether TBR1 influences expression of these genes in the amygdala, we carried out quantitative PCR using amygdalar RNAs. We found that mRNA expression of *Ntng1* and *Cdh8* was upregulated in both the adult and one-day-old (P1) *Tbr1*$^{+/-}$ amygdalae, whereas the expression of *Cntn2* was downregulated (**Fig. 2d**,**e**), indicating that they are also regulated by TBR1 in the amygdala.

We then investigated whether TBR1 controls axonal outgrowth of amygdalar neurons through the aforementioned target genes. First, compared with wild-type amygdalar neurons, *Tbr1*$^{+/-}$ amygdalar neurons developed multiple axons and each axon was shorter at 4 days *in vitro* (DIV) (**Fig. 3a**). Overexpression of wild-type TBR1 rescued these axonal defects (**Fig. 3a**), supporting the role of *Tbr1* in regulation of amygdalar axonal growth and differentiation. We also investigated whether the mutations in the *TBR1* gene identified in patients with ASDs influence the ability of TBR1 to regulate axon growth. Four mutations in the *TBR1* gene have been identified in patients[6,7,10]. Two of them are expected to express truncated proteins. The other two mutants have missense mutations, N374H and K228E. On the basis of the structure of the T-box of Brachury[21], the prototype T-box protein, the residue K228 is predicted to directly interact with DNA; the residue N374 is adjacent to the DNA-binding residue. We introduced the N374H substitution into mouse TBR1 and found that the TBR1 N374H mutant did not rescue the axonal defects of *Tbr1*$^{+/-}$ amygdalar neurons (**Fig. 3a**), suggesting that the ability to control axonal growth and differentiation is lost in the N374H mutant.

The axonal phenotypes of *Tbr1*$^{+/-}$ neurons were also examined at 7 and 10 DIV. Similarly to those observed at 4 DIV, the axons of *Tbr1*$^{+/-}$ neurons were not effectively extended (**Fig. 3b** and SMI-312 immunostaining data not shown). We also noticed that axon outgrowth and differentiation of *Tbr1*$^{-/-}$ neurons were similar to those of *Tbr1*$^{+/-}$ neurons (**Fig. 3b**). Thus, loss of one *Tbr1* allele is sufficient to induce the axon defects in amygdalar neurons.

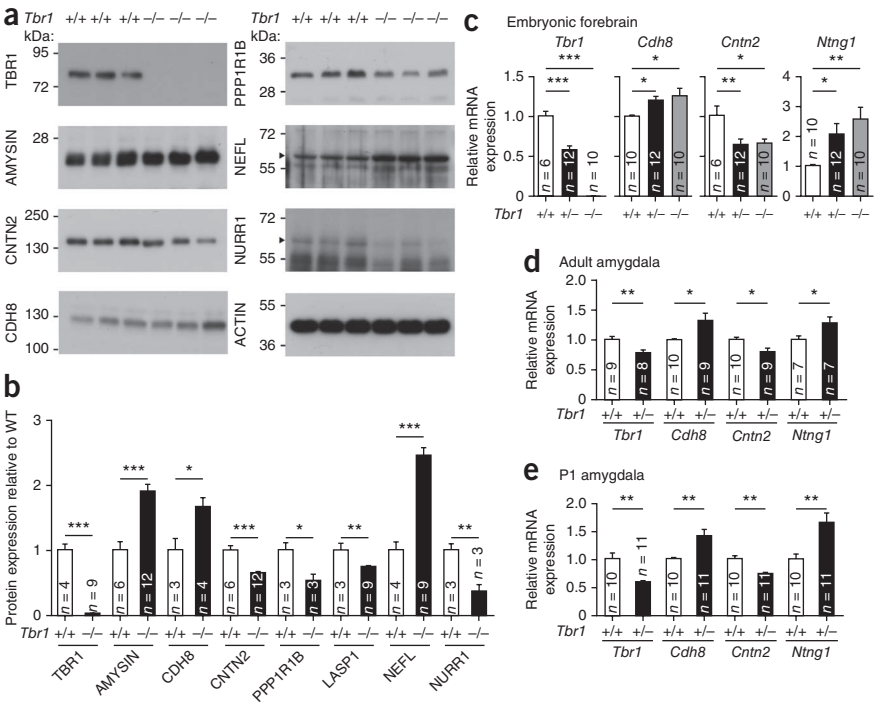

Figure 2 Immunoblotting and quantitative PCR confirm alteration of gene expression in *Tbr1*-deficient mice. (**a**) Immunoblots using the total forebrain extracts prepared from embryonic day 16.5 (E16.5) mice. Full-length blots are presented in **Supplementary Figure 9**. (**b**) Quantification of the immunoblots. The results were normalized against ACTIN. The protein expression of CNTN2, PPP1R1B, LASP1 and NURR1 was downregulated in $Tbr1^{+/-}$ mice, whereas expression of AMYSIN, CDH8 and NEFL was upregulated in $Tbr1^{+/-}$ mice. (**c**–**e**) Quantitative-PCR analyses of *Cdh8*, *Ntng1* and *Cntn2* in the E16.5 forebrain (**c**), adult amygdala (**d**) and P1 amygdala (**e**). All data are presented as the mean plus s.e.m. The animal sample sizes (*n*) for each experiment are indicated in the figures. Multiple comparisons with Dunnett test were performed for data shown in **c**. (**b**) TBR1 $P < 0.001$, $t = 18$, d.f. = 11; AMYSIN $P < 0.001$, $t = 5.254$, d.f. = 16; CDH8 $P = 0.027$, $t = 3.096$, d.f. = 5; CNTN2 $P < 0.001$, $t = 4.769$, d.f. = 16; PPP1R1B $P = 0.029$, $t = 3.345$, d.f. = 4; LASP1 $P = 0.005$, $t = 3.559$, d.f. = 10; NEFL $P < 0.001$, $t = 7.339$, d.f. = 11; NURR1 $P = 0.009$, $t = 4.739$, d.f. = 4. (**c**) *Tbr1*: $Tbr1^{+/+}$ vs. $Tbr1^{+/-}$ $P < 0.001$, $Tbr1^{+/+}$ vs. $Tbr1^{-/-}$ $P < 0.001$, d.f. = 27, $F = 121.8$; Cdh8: $Tbr1^{+/+}$ vs. $Tbr1^{+/-}$ $P = 0.046$, $Tbr1^{+/+}$ vs. $Tbr1^{-/-}$ $P = 0.015$, d.f. = 31, $F = 4.579$; Cntn2: $Tbr1^{+/+}$ vs. $Tbr1^{+/-}$ $P = 0.006$, $Tbr1^{+/-}$ vs. $Tbr1^{-/-}$ $P = 0.01$, d.f. = 27, $F = 5.998$; Ntng1: $Tbr1^{+/+}$ vs. $Tbr1^{+/-}$ $P = 0.047$, $Tbr1^{+/+}$ vs. $Tbr1^{-/-}$ $P = 0.004$, d.f. = 31, $F = 5.836$. (**d**) *Tbr1* $P = 0.0096$, d.f. = 15, $t = 2.967$; *Cdh8* $P = 0.0191$, d.f. = 17, $t = 2.590$; *Cntn2* $P = 0.0154$, d.f. = 17, $t = 2.694$; *Ntng1* $P = 0.0435$, d.f. = 12, $t = 2.257$. (**e**) *Tbr1* $P = 0.0021$, d.f. = 19, $t = 3.555$; *Cdh8* $P = 0.007$, d.f. = 19, $t = 3.024$; *Cntn2* $P = 0.0022$, d.f. = 19, $t = 3.539$; *Ntng1* $P = 0.0052$, d.f. = 19, $t = 3.153$. $^*P < 0.05$; $^{**}P < 0.01$; $^{***}P < 0.001$.

We then examined whether manipulation of TBR1 target genes has a beneficial effect on axonal differentiation of $Tbr1^{+/-}$ amygdalar neurons. The expression of miR-Ntng1 and miR-Cdh8 as well as *Cntn2* in $Tbr1^{+/-}$ amygdalar neurons promoted axonal growth and reduced the percentage of multipolar neurons (**Fig. 3c**). Knockdown of either *Cdh8* or *Ntng1* effectively rescued the multipolarity phenotype. However, miR-Ntng1 was more effective on axon length than miR-Cdh8 (**Fig. 3c**), suggesting that NTNG1, CDH8 and CNTN2 likely have overlapping but not identical functions in regulation of axonal phenotypes.

TBR1 regulates axonal projection of the amygdala *in vivo*

We further investigated the morphological characteristics of amygdalar neurons *in vivo* using *in utero* electroporation (IUE). In wild-type mice, when the GFP construct was successfully transfected into the amygdala, the anterior commissure was clearly labeled by GFP signals (**Fig. 4**). In contrast, we did not see GFP-positive signals in the anterior commissure in $Tbr1^{+/-}$ embryos with successful amygdala transfection (**Fig. 4**), consistent with the loss of the posterior anterior commissure in $Tbr1^{+/-}$ adult mice (**Fig. 1a**,**b**). We then transfected the miR-Ntng1, miR-Cdh8 and *Cntn2* expression constructs into $Tbr1^{+/-}$ embryos. When these constructs were successfully delivered into the amygdala of $Tbr1^{+/-}$ embryo, GFP-positive axons clearly extended to the position of anterior commissure and crossed the midline (**Fig. 4**), indicating that downregulation of *Ntng1* and *Cdh8* and upregulation of *Cntn2* in $Tbr1^{+/-}$ amygdala promoted axonal extension of the amygdala to the anterior commissure. These GFP-positive axons were in the posterior part of anterior commissure and were extended from the amygdala (see the detailed explanation in the legend of **Supplementary Fig. 6**). These findings suggest that manipulating the expression of TBR1 target genes in $Tbr1^{+/-}$ mice promotes axonal projection of amygdalar neurons to the anterior commissure.

We also examined the morphology of amygdalar neurons in the electroporated embryos. Wild-type neurons extended long processes from the soma. However, we rarely found long processes extending from $Tbr1^{+/-}$ amygdalar neurons (**Supplementary Fig. 6c**). Knockdown of *Cdh8* and *Ntng1* and overexpression of *Cntn2* resulted in $Tbr1^{+/-}$ amygdalar neurons with morphology more similar to that of the wild-type neurons (**Supplementary Fig. 6c**). We also found that, in contrast to that of the amygdalar neurons, the morphology of $Tbr1^{+/-}$ cortical and striatal neurons was comparable to wild-type neurons (**Supplementary Fig. 6c**). These *in vivo* data further suggest that TBR1 and its target genes have roles in differentiation of amygdalar neurons.

Tbr1$^{+/-}$ mice show abnormal behaviors

Because the amygdala circuitry seems to be defective in $Tbr1^{+/-}$ mice, we next investigated whether *Tbr1* haploinsufficiency results in abnormal behaviors. $Tbr1^{+/-}$ mice showed no obvious deficits in open-field and elevated plus-maze tests (**Supplementary Fig. 7a**,**b**), indicating no deficiency in locomotion or anxiety. We then conducted learning and memory tests. In the conditioned taste aversion (CTA) test (**Supplementary Fig. 7h**), both $Tbr1^{+/-}$ mice and wild-type littermates showed a preference to drink sucrose solution on the training day (**Fig. 5a**). After training with LiCl injection, $Tbr1^{+/-}$ mice did not recognize sucrose as a hazardous food and drank more sucrose than water (**Fig. 5b**), indicating impairment in CTA. In addition, $Tbr1^{+/-}$ mice also had defective auditory fear conditioning

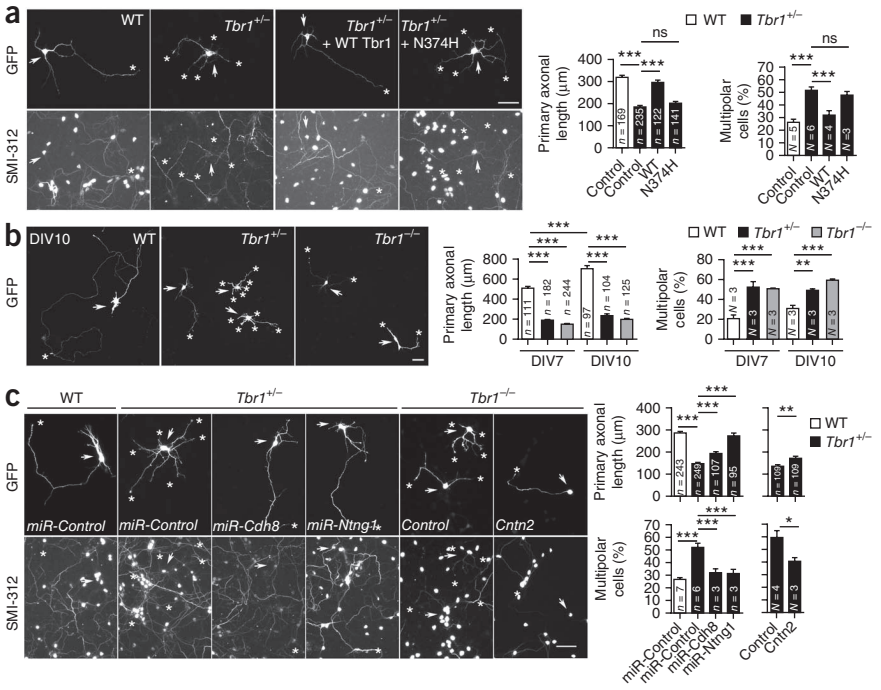

Figure 3 Axonal defects of *Tbr1*$^{+/-}$ amygdalar neurons are rescued by expression of wild-type *Tbr1* and manipulation of the *Ntng1*, *Cntn2* and *Cdh8* expression. (**a**) *Tbr1* haploinsufficiency shortened the axonal length and induced multi-axon formation in cultured amygdalar neurons. Overexpression of wild-type *Tbr1*, but not the N374H mutant, rescued the axonal phenotypes in *Tbr1*$^{+/-}$ neurons. Cultured amygdalar neurons were transfected with indicated plasmids at 2 DIV and fixed for immunostaining at 4 DIV. (**b**) Axonal defects of *Tbr1*$^{+/-}$ amygdalar neurons were still preserved at 7 and 10 DIV. Transfection was performed at 4 DIV and immunostaining was carried out at 7 and 10 DIV, as indicated, although only the 10 DIV data are shown. (**c**) Knockdown of *Cdh8* or *Ntng1* or overexpression of *Cntn2* rescued the axonal defects caused by *Tbr1* haploinsufficiency. Cultured amygdalar neurons were transfected with indicated plasmids at 2 DIV and fixed for immunostaining at 4 DIV. The GFP signals were used to outline the cell morphology. Double immunolabeling with axonal marker SMI-312 was performed to confirm axonal identity. Asterisks label the SMI-312-positive processes. The longest SMI-312-positive process of a neuron is defined as the primary axon. All data are presented as the mean plus s.e.m. The sample sizes (*n*) for each experiment and the number of times (*N*) each experiment was conducted are indicated in the figure. (**a**) Length: *Tbr1*$^{+/+}$ control vs. *Tbr1*$^{+/-}$ control $P < 0.001$; *Tbr1*$^{+/-}$ control vs. *Tbr1*$^{+/-}$ + WT $P < 0.001$; *Tbr1*$^{+/-}$ control vs. *Tbr1*$^{+/-}$ + N374H $P = 0.384$; d.f. = 666, F(genotype) = 176.664, F(O/E) = 51.723. Multipolar: *Tbr1*$^{+/+}$ control vs. *Tbr1*$^{+/-}$ control $P < 0.001$; *Tbr1*$^{+/-}$ control vs *Tbr1*$^{+/-}$ + WT $P < 0.001$; *Tbr1*$^{+/-}$ control vs *Tbr1*$^{+/-}$ + N374H $P = 1.000$; d.f. = 17, F(genotype) = 46.249, F(O/E) = 12.652. (**b**) Length: DIV7 vs. DIV10 (within *Tbr1*$^{+/+}$) $P < 0.001$; *Tbr1*$^{+/+}$ vs. *Tbr1*$^{+/-}$ (within DIV7 and DIV10) $P < 0.001$; *Tbr1*$^{+/+}$ vs. *Tbr1*$^{-/-}$ (within DIV7 and DIV10): $P < 0.001$; d.f. = 862, F(genotype) = 518.641, F(DIV) = 69.209. Multipolar: *Tbr1*$^{+/+}$ vs. *Tbr1*$^{+/-}$ (within DIV7 and DIV10) $P < 0.001$; *Tbr1*$^{+/+}$ vs. *Tbr1*$^{-/-}$ (within DIV7) $P < 0.001$; *Tbr1*$^{+/+}$ vs. *Tbr1*$^{-/-}$ (within DIV10) $P < 0.001$; d.f. = 17, F(genotype) = 51.432, F(DIV) = 3.850. (**c**) Length miR: *Tbr1*$^{+/+}$ vs. *Tbr1*$^{+/-}$ (within control) $P < 0.001$; Control vs. miR-Cdh8 (within *Tbr1*$^{+/-}$) $P < 0.001$; Control vs. miR-Ntng1 (within *Tbr1*$^{+/-}$) $P < 0.001$; d.f. = 693, F(genotype) = 218.680, F(O/E) = 50.658. Length *Cntn2*: $P = 0.0045$, d.f. = 216, $t = 2.874$. Multipolar miR: *Tbr1*$^{+/+}$ vs. *Tbr1*$^{+/-}$ (within control) $P < 0.001$; Control vs. miR-Cdh8 (within *Tbr1*$^{+/-}$) $P < 0.001$; Control vs. miR-Ntng1 (within *Tbr1*$^{+/-}$) $P < 0.001$; d.f. = 18, F(genotype) = 60.011, F(O/E) = 18.180. Multipolar Cntn2: $P = 0.0432$, d.f. = 5, $t = 2.692$. Scale bars: 50 μm (**a**–**c**). *$P < 0.05$; **$P < 0.01$; ***$P < 0.001$.

(AFC), showing a lower freezing response when examined for auditory fear memory (**Fig. 5c**). In contrast to their performance in the CTA and AFC tests, the behavior of *Tbr1*$^{+/-}$ mice was similar to that of their wild-type littermates in novel object recognition and contextual fear conditioning (**Supplementary Fig. 7c**,**d**). These results suggest that some associative memory was impaired in *Tbr1*$^{+/-}$ mice.

We then used the appetitive-motivated T-maze test and two-choice digging test to analyze the cognitive flexibility of *Tbr1*$^{+/-}$ mice. In the T-maze, wild-type and *Tbr1*$^{+/-}$ mice took a similar amount of time to learn (**Fig. 5d**). However, in reversal learning, the *Tbr1*$^{+/-}$ mice took a longer amount of time to realize that the reward had been changed to the other arm in the T-maze (**Fig. 5e**). The results were similar in the two-choice digging test. The ability of *Tbr1*$^{+/-}$ mice to find food embedded in original sawdust was comparable with that of wild-type mice (**Fig. 5f**). However, *Tbr1*$^{+/-}$ mice took considerably more trials to relearn that food had been moved to the bowl filled with cinnamon-flavored sawdust (**Fig. 5g**). Together, these results suggest impairment in cognitive flexibility in *Tbr1*$^{+/-}$ mice.

To study whether TBR1 also influences social behaviors and communication, we carried out four further assays. In the three-chamber test, *Tbr1*$^{+/-}$ mice showed deficits in sociability (**Fig. 5h**), but not preference for social novelty (**Fig. 5i**). In a test of reciprocal social interaction, *Tbr1*$^{+/-}$ mice also spent much less time interacting with unfamiliar mice (**Fig. 5j**). In the assay for social transmission of food preference, wild-type mice interacted with the demonstrator and preferred the cued food (cinnamon-flavored food), which had been eaten by the demonstrator. In contrast, *Tbr1*$^{+/-}$ mice did not show a preference for the cued food (**Fig. 5k**). This difference was not due to the preference of *Tbr1*$^{+/-}$ mice for another flavor (cocoa in our experiments), because both *Tbr1*$^{+/-}$ mice and wild-type littermates refused to eat both of the flavored foods in the absence of cues from the demonstrator (**Fig. 5l**). The last behavioral paradigm used involved the monitoring of ultrasonic vocalizations. When pups were isolated from their mothers, *Tbr1*$^{+/-}$ pups produced much fewer ultrasonic vocalization emissions compared with wild-type littermates (**Fig. 5m**), indicating a communication deficit in *Tbr1*$^{+/-}$ mice. Together, these behavioral analyses indicate that *Tbr1* haploinsufficiency results in impairment of associative memory, social interaction, communication and cognitive flexibility.

Activation of *Tbr1*$^{+/-}$ amygdalar neurons is aberrant

The impairment of axonal connections between and within amygdalae likely damages neuronal activation of the amygdala in *Tbr1*$^{+/-}$ mice upon behavioral stimulation. To examine this possibility, we counted c-FOS–positive cells following CTA and AFC. In the *Tbr1*$^{+/-}$ lateral amygdala, the number of c-FOS–positive cells was much lower than that in wild-type littermates (**Fig. 6a–d**). In the basal amygdala, a difference was found only after CTA (**Fig. 6a–d**). The differences were unlikely due to a lower cell density in the *Tbr1*$^{+/-}$ amygdala because the cell density was similar between the wild-type and *Tbr1*$^{+/-}$ amygdalae

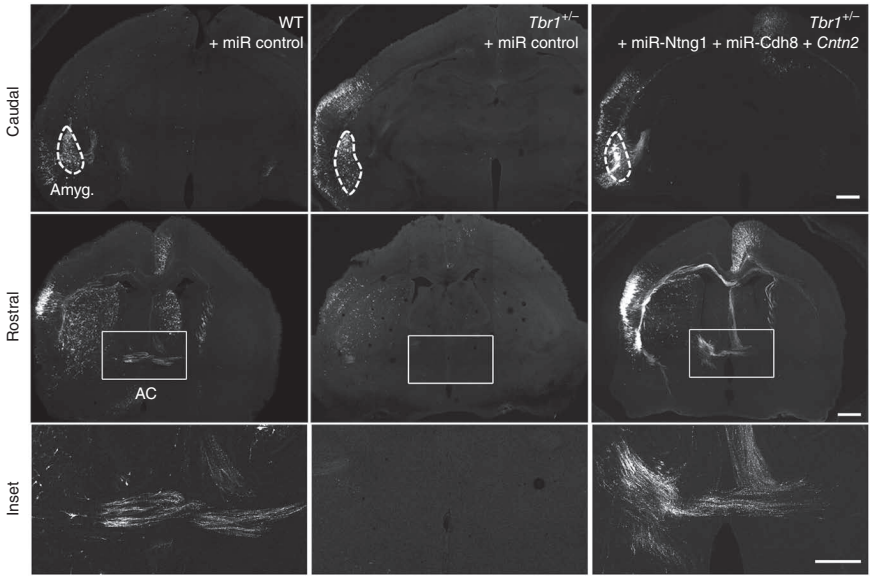

Figure 4 TBR1 and its target genes are critical for anterior commissure *in vivo*. IUE with GFP expression construct was performed at E12.5–13.5 and immunostaining was then carried out at E18.5–19.5. In addition to transfecting control GFP vector into wild-type and *Tbr1*$^{+/-}$ embryos, we triply transfected constructs for miR-Ntng1, miR-Cdh8 and *Cntn2* into *Tbr1*$^{+/-}$ embryos. Coronal sections at the caudal part show the amygdala region circled with a dashed line; sections at rostral part indicate the anterior commissure. The bottom images are enlarged images of the insets containing the anterior commissure. GFP vector was successfully transfected into the amygdala of four wild-type and three *Tbr1*$^{+/-}$ embryos. For *Tbr1*$^{+/-}$ embryos transfected with miR-Ntng1, miR-Cdh8 and *Cntn2* constructs, five successful cases were obtained. Only one representative image for each group is shown here. In these successful cases, all of wild-type and rescue groups had a GFP-positive anterior commissure. For animals without amygdala labeling, there was no GFP signal at anterior commissure. Those data are summarized in **Supplementary Figure 6**. Scale bars: caudal and rostral, 500 μm; inset, 200 μm.

(**Supplementary Fig. 5f**,**g**). In contrast to what we observed in the amygdala, the number of c-FOS–positive cells in the hippocampus was comparable between *Tbr1*$^{+/-}$ mice and wild-type littermates after CTA and AFC (**Fig. 6e**–**h**). The c-FOS–positive cells were mainly TBR1-positive neurons (**Fig. 6i**), indicating that TBR1-positive projection neurons are the major population activated during CTA and AFC.

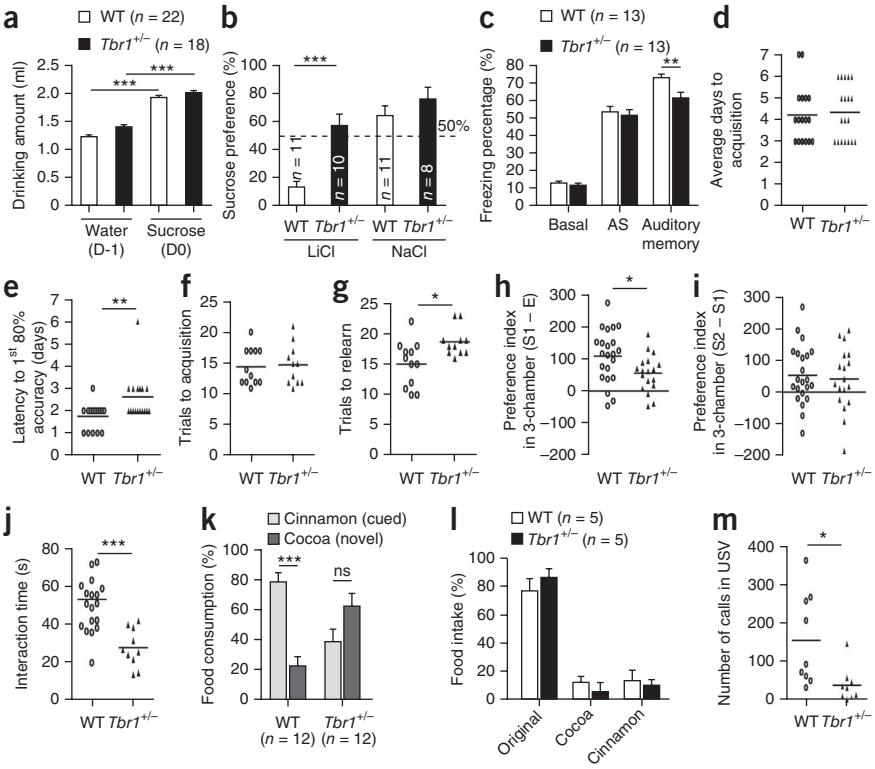

Figure 5 *Tbr1* haploinsufficiency results in autism-like behaviors in mice. (**a**) The amount of water intake during pretraining (D-1) and the amount of sucrose intake on the CTA training day (D0). (**b**) The results of the two-bottle sucrose preference test in CTA. A sucrose preference index higher than 50% indicates the impairment in CTA. (**c**) Auditory fear conditioning. The freezing responses of the mice before electric shock (basal), immediately after the third electric shock (AS) and one day after training (auditory fear memory) are shown. (**d**) The average days for acquisition in the T-maze. (**e**) The latency to achieve 80% accuracy in reversal learning in the T-maze. (**f**) Acquisition in the two-choice digging task was comparable between wild-type and *Tbr1*$^{+/-}$ mice. (**g**) *Tbr1*$^{+/-}$ mice needed more trials to relearn in the two-choice digging test. (**h**) *Tbr1*$^{+/-}$ mice showed lower sociability in the three-chamber test. (**i**) The novelty preference was normal in *Tbr1* mutant mice in the three-chamber test. (**j**) Reduced reciprocal social interactions in *Tbr1*$^{+/-}$ mice. (**k**) *Tbr1* mutant mice were defective in the social transmission of food preference because they showed no preference for either the cued or novel foods. (**l**) Both the wild-type and *Tbr1* mutant mice avoided the cinnamon- and cocoa-flavored food in the absence of information from the demonstrators. (**m**) Lower frequency of ultrasonic vocalizations in isolated *Tbr1*$^{+/-}$ pups. (**a**–**c**, **k**–**l**) The animal sample sizes (*n*) for each experiment are indicated in each panel. Data are presented as the mean plus s.e.m. (**d**–**j**, **m**) Each dot indicates the results obtained from an individual animal. The horizontal lines represent the means. (**a**) Water vs. sucrose (within *Tbr1*$^{+/+}$ or *Tbr1*$^{+/-}$) $P < 0.001$, d.f. = 79, F(genotype) = 12.665, F(treatment) = 314.291. (**b**) *Tbr1*$^{+/+}$ vs. *Tbr1*$^{+/-}$ (within LiCl) $P < 0.001$, d.f. = 39, F(genotype) = 16.484, F(treatment) = 26.257. (**c**) *Tbr1*$^{+/+}$ vs. *Tbr1*$^{+/-}$ (auditory memory) $P = 0.0054$, d.f. = 24, $t = 3.055$. (**d**) $P = 0.7568$, d.f. = 34, $t = 0.3122$. (**e**) $P = 0.0025$, d.f. = 34, $t = 3.26$. (**f**) $P = 0.8067$, d.f. = 21, $t = 0.2478$. (**g**) $P = 0.0109$, d.f. = 21, $t = 2.793$. (**h**) $P = 0.0257$, d.f. = 38, $t = 2.321$. (**i**) $P = 0.7020$, d.f. = 38, $t = 0.3856$. (**j**) $P < 0.001$, d.f. = 28, $t = 4.408$. (**k**) *Tbr1*$^{+/+}$ $P < 0.001$, d.f. = 22, $t = 6.327$; *Tbr1*$^{+/-}$ $P = 0.0581$, d.f. = 22, $t = 1.999$. (**l**) *Tbr1*$^{+/+}$: original vs. cocoa $P < 0.001$, original vs. cinnamon $P < 0.001$, d.f. = 14, $F = 141.1$; *Tbr1*$^{+/-}$: original vs. cocoa $P < 0.001$, original vs. cinnamon $P < 0.001$, d.f. = 14, $F = 330.4$. (**m**) $P = 0.0145$, d.f. = 16, $t = 2.742$. *$P < 0.05$; **$P < 0.01$; ***$P < 0.001$.

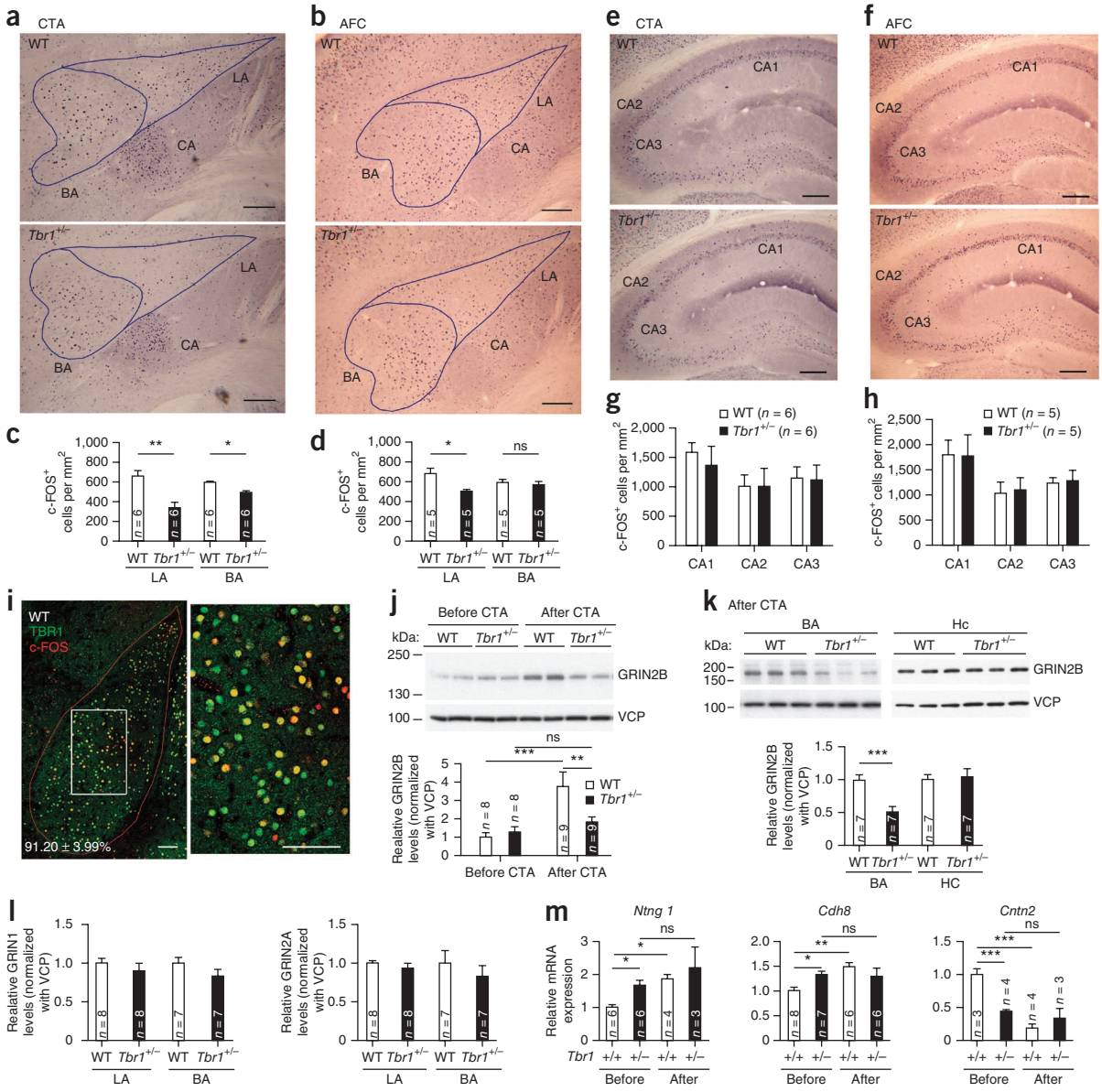

Figure 6 Neuronal activation in the amygdala is impaired in *Tbr1*$^{+/-}$ mice. (**a**–**h**) The c-FOS expression in wild-type and *Tbr1*$^{+/-}$ amygdalae. Two hours after CTA (**a**, **c**, **e**, **g**) or AFC (**b**, **d**, **f**, **h**), the mouse brains were fixed for immunostaining with c-FOS antibodies. The c-FOS–positive cells in the basal and lateral amygdala and the CA1, CA2 and CA3 of hippocampus are shown. Panels **c**, **d**, **g** and **h** are the quantifications of panels **a**, **b**, **e** and **f**, respectively. (**i**) After CTA training, activated amygdalar neurons indicated by c-FOS immunoreactivities are mainly TBR1-positive projection neurons in wild-type mice. Double immunostaining with TBR1 and c-FOS antibodies was carried out two hours after CTA training. The right panel is an enlarged image of the inset. c-FOS and TBR1 double-positive cells as a percentage of the total c-FOS-positive cells in the amygdala (outlined in red) are indicated. The data are presented as the means ± s.e.m. of three mice. (**j**) GRIN2B protein expression in the lateral amygdala was upregulated in the wild-type mice, but not in the *Tbr1*$^{+/-}$ mice after CTA training. (**k**) After CTA, GRIN2B expression was lower in *Tbr1*$^{+/-}$ basal amygdala compared with wild-type basal amygdala. Note that GRIN2B expression in the hippocampus was not changed. For **j** and **k**, full-length blots are presented in **Supplementary Figure 9**. (**l**) Expression of GRIN1 and GRIN2A in the amygdala was not altered after CTA. (**m**) Quantitative-PCR analysis of *Ntng1*, *Cdh8* and *Cntn2* before and after CTA training. The changes in wild-type and *Tbr1*$^{+/-}$ amygdalae were compared. Scale bars: 200 μm (**a**,**b**,**e**,**f**); 100 μm (**i**). The sample sizes (*n*) for each experiment are indicated in the figure. All data are presented as the mean plus s.e.m. (**c**) LA $P = 0.0028$, df = 10, $t = 3.933$; BA $P = 0.0106$, df = 10, $t = 3.136$. (**d**) LA $P = 0.0174$, d.f. = 8, $t = 2.989$; BA $P = 0.5256$, d.f. = 8, $t = 0.6635$. (**g**) *Tbr1*$^{+/+}$ vs. *Tbr1*$^{+/-}$ (within CA1) $P = 0.127$; *Tbr1*$^{+/+}$ vs. *Tbr1*$^{+/-}$ (within CA2) $P = 0.898$; *Tbr1*$^{+/+}$ vs. *Tbr1*$^{+/-}$ (within CA3) $P = 0.741$; d.f. = 35, F(genotype) = 1.375, F(area) = 10.35. (**h**) *Tbr1*$^{+/+}$ vs. *Tbr1*$^{+/-}$ (within CA1) $P = 0.857$; *Tbr1*$^{+/+}$ vs. *Tbr1*$^{+/-}$ (within CA2) $P = 0.731$; *Tbr1*$^{+/+}$ vs. *Tbr1*$^{+/-}$ (within CA3) $P = 0.874$; d.f. = 29, F(genotype) = 0.0354, F(area) = 17.918. (**j**) Before vs. after (within *Tbr1*$^{+/+}$) $P < 0.001$; before vs. after (within *Tbr1*$^{+/-}$) $P = 0.427$; *Tbr1*$^{+/+}$ vs. *Tbr1*$^{+/-}$ (within after) $P = 0.007$; d.f. = 33, F(genotype) = 3.072, F(treatment) = 11.483. (**k**) BA $P < 0.001$, d.f. = 12, $t = 5.738$; Hc $P = 0.8498$, d.f. = 12, $t = 0.1935$. (**l**) GRIN1/LA $P = 0.3702$, d.f. = 14, $t = 0.9258$; GRIN1/BA $P = 0.1642$, d.f. = 12, $t = 1.482$; GRIN2A/LA $P = 0.3596$, d.f. = 14, $t = 0.9471$; GRIN2A/BA $P = 0.4162$, d.f. = 12, $t = 0.8421$. (**m**) *Ntng1*: *Tbr1*$^{+/+}$ vs. *Tbr1*$^{+/-}$ (within before) $P = 0.043$; before vs. after (within *Tbr1*$^{+/+}$) $P = 0.018$; before vs. after (within *Tbr1*$^{+/-}$) $P = 0.157$; d.f. = 26, F(genotype) = 0.244, F(treatment) = 4.384. *Cdh8*: *Tbr1*$^{+/+}$ vs. *Tbr1*$^{+/-}$ (within before) $P = 0.038$; before vs. after (within *Tbr1*$^{+/+}$) $P = 0.003$; before vs. after (within *Tbr1*$^{+/-}$) $P = 0.809$; d.f. = 26, F(genotype) = 0.244, F(treatment) = 4.384. *Cntn2*: *Tbr1*$^{+/+}$ vs. *Tbr1*$^{+/-}$ (within before) $P < 0.001$; before vs. after (within *Tbr1*$^{+/+}$) $P < 0.001$; before vs. after (within *Tbr1*$^{+/-}$) $P = 0.414$; d.f. = 13, F(genotype) = 5.719, F(treatment) = 27.301. $^*P < 0.05$; $^{**}P < 0.01$; $^{***}P < 0.001$.

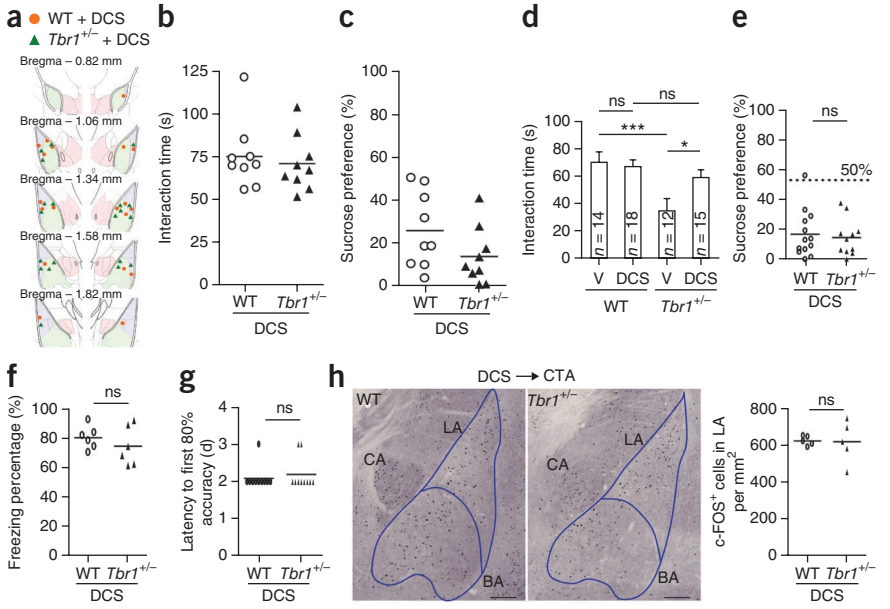

Figure 7 Administration of D-cycloserine ameliorates the behavioral defects in *Tbr1*$^{+/-}$ mice. (**a**–**c**) D-Cycloserine (DCS) were bilaterally infused into the basolateral amygdala. (**d**–**h**) Administration of DCS via intraperitoneal injection. Thirty minutes after DCS injection, animals were subjected to behavioral analyses. (**a**) Infusion sites at amygdalae. (**b**,**d**) Reciprocal social interaction. (**c**,**e**) Sucrose preference in CTA. (**f**) AFC memory. (**g**) Cognitive inflexibility in the T-maze. (**h**) Neuronal activation as assessed by c-FOS expression after CTA. V, vehicle control; DCS, D-Cycloserine. Each dot in panels **b**–**c** and **e**–**h** indicates the results obtained from an individual animal. The horizontal lines represent the means. The animal sample sizes (*n*) for each experiment are indicated in panel **d**. All data are presented as the mean plus s.e.m. (**b**) $P = 0.632$, $t = 0.4883$, d.f. = 16. (**c**) $P = 0.122$, $t = 1.635$, d.f. = 16. (**d**) *Tbr1*$^{+/+}$ vs. *Tbr1*$^{+/-}$ (within V) $P < 0.001$; *Tbr1*$^{+/+}$ vs. *Tbr1*$^{+/-}$ (within D) $P = 0.333$; V vs. D (within *Tbr1*$^{+/+}$) $P = 0.793$; V vs. D (within *Tbr1*$^{+/-}$) $P = 0.020$; d.f. = 58, F(genotype) = 10.534, F(treatment) = 2.427. (**e**) $P = 0.7015$, d.f. = 22, $t = 0.3884$. (**f**) $P = 0.3871$, d.f. = 10, $t = 0.9042$. (**g**) $P = 0.5560$, d.f. = 18, $t = 0.6$. (**h**) $P = 0.9314$, d.f. = 8, $t = 0.08887$. $^*P < 0.05$; $^{***}P < 0.001$. ns, not significant. Scale bars: 100 μm.

We then examined the expression of TBR1 target genes in the amygdala after behavioral stimulation. Because GRIN2B is highly relevant to neuronal activity, its expression was examined first. Before CTA, GRIN2B expression in the lateral amygdala was unchanged in *Tbr1*$^{+/-}$ mice compared to wild-type littermates (**Fig. 6j**). After CTA, the GRIN2B protein expression in the wild-type showed an increase in the lateral amygdala; however, there was no induction of GRIN2B expression in *Tbr1*$^{+/-}$ mice (**Fig. 6j**). GRIN2B expression in the wild-type was also higher than that in *Tbr1*$^{+/-}$ mice in the basal amygdala after CTA (**Fig. 6k**). In contrast to GRIN2B expression in the amygdala, GRIN2B expression in the hippocampus was comparable in wild-type and *Tbr1*$^{+/-}$ mice after CTA (**Fig. 6k**). In addition, we did not observe any changes in GRIN2A and GRIN1 expression when we compared wild-type littermates and *Tbr1*$^{+/-}$ mice after CTA (**Fig. 6l**). These results suggest that GRIN2B induction was impaired in the *Tbr1*$^{+/-}$ amygdala after behavioral stimulation.

We also investigated the expression of *Ntng1*, *Cdh8* and *Cntn2* in the amygdala upon behavioral stimulation. After behavioral training, the expression of *Ntng1* and *Cdh8* was upregulated in the wild-type amygdala, whereas expression of *Cntn2* was downregulated (**Fig. 6m**). It seems possible that these genes are involved in remodeling after neuronal activation. In *Tbr1*$^{+/-}$ mice, none of these genes was altered by behavioral stimulation (**Fig. 6m**), suggesting that regulation of these genes by neuronal activation is also aberrant in *Tbr1*$^{+/-}$ mice.

D-Cycloserine ameliorates the defects of *Tbr1*$^{+/-}$ mice

Because the experiments outlined above suggested that neuronal activation at the amygdala is impaired in *Tbr1*$^{+/-}$ mice, we then investigated whether increasing the activity of amygdalar neurons is able to ameliorate the behavioral defects observed in *Tbr1*$^{+/-}$ mice. D-Cycloserine, a partial agonist of NMDA receptors (NMDARs)[22,23] was directly infused into the basolateral amygdala of *Tbr1*$^{+/-}$ mice 30 min before behavioral assays (**Fig. 7a**). We found that this treatment effectively ameliorated the social interaction and CTA defects in *Tbr1*$^{+/-}$ mice (**Fig. 7b**,**c**), suggesting that increase of amygdalar NMDAR activity ameliorated the behavioral defects of *Tbr1*$^{+/-}$ mice. We also infused ifenprodil, a GRIN2B antagonist, into the amygdalae of wild-type mice (**Supplementary Fig. 7e**) and found that local inhibition of amygdalar activity by ifenprodil impaired reciprocal social interaction and associative memory of CTA (**Supplementary Fig. 7f**,**g**). This finding is consistent with previous studies that found that amygdalar NMDAR activity is important in fear memory, one well-studied function of the amygdala[24,25].

In addition to local infusion, D-cycloserine was also intraperitoneally injected into both wild-type and *Tbr1*$^{+/-}$ mice. Compared with vehicle control, D-cycloserine noticeably improved the reciprocal social interaction of *Tbr1*$^{+/-}$ mice to a level comparable to that of wild-type littermates (**Fig. 7d**). D-Cycloserine treatment also effectively ameliorated the defects of *Tbr1*$^{+/-}$ mice in associative memory, as shown by CTA as well as AFC (**Fig. 7e**,**f**), and in cognitive flexibility, as shown by the T-maze test (**Fig. 7g**). Consistent with this, D-cycloserine treatment also increased the number of c-FOS–positive cells in the lateral amygdala of *Tbr1*$^{+/-}$ mice after behavioral stimulation (**Fig. 7h**). Because D-cycloserine binds to the glycine$_B$ site of the NMDAR, the function of D-cycloserine is to promote efficient opening of NMDAR in the presence of glutamate. D-Cycloserine did not alter the expression levels of GRIN2B as well as other TBR1 target genes (**Supplementary Fig. 8a**–**d**). Together, these results suggest that systemic treatment with D-cycloserine that increases neuronal activity also ameliorates the behavioral defects observed in *Tbr1*$^{+/-}$ mice.

DISCUSSION

In this report, we provide evidence that *Tbr1* haploinsufficiency results in the impairment of both inter- and intra-amygdalar axonal projections. TBR1 acts cell-autonomously to regulate the expression of various downstream target genes, including *Ntng1*, *Cdh8* and *Cntn2*, and to control amygdalar axonal growth. Because *Tbr1* and these genes are also expressed in the cerebral cortex, it is not clear why the amygdala is particularly sensitive to *Tbr1* haploinsufficiency. Perhaps unknown region-specific factors in the cerebral cortex or amygdala influence the outcome of *Tbr1* haploinsufficiency.

TBR1 has been reported to highly associate with ASDs[10]. However, it was unclear whether mutations in this gene induce autistic characteristics. Using *Tbr1*$^{+/-}$ mice as a model, we demonstrated that in addition to the axonal defects observed in the amygdala, loss of one *Tbr1* allele is sufficient to induce cognitive abnormality in mice. Social interaction, cognitive flexibility and associative memory are defective in *Tbr1*$^{+/-}$ mice. The characteristics of these behavioral defects are similar to those in patients with autism. Our study, therefore, strengthens the evidence for the role of *TBR1* in psychiatric disorder.

Although our data suggest that the behavioral defects in *Tbr1*$^{+/-}$ mice resemble the characteristics of patients with autism and that *Tbr1*$^{+/-}$ mice show structural and functional impairments of amygdala, we do not wish to assert that the amygdala is the sole controller of autism-related behavior. Current understanding about autism purports that "miswiring" or "misprocessing" of information in the brain is a feature of ASDs. Therefore, no matter which brain region is affected, as long as the region is involved in information processing of autism-related behaviors, local defects in the region will likely induce abnormal behaviors. This can explain why hundreds of genes, as well as all of the cerebral cortex, hippocampus, striatum, amygdala and cerebellum, are associated with ASDs. Because the amygdala is known to connect to the cerebral cortex, hippocampus, striatum and brain stem, defects in the amygdala may impair information processing within the amygdala and between the amygdala and other brain regions, thus resulting in abnormal behaviors. In addition, although here we focus on the amygdalar defects in *Tbr1*$^{+/-}$ mice, it is possible that impairment in the other brain regions may also be involved in the abnormal behaviors of *Tbr1*$^{+/-}$ mice. More investigations are needed to address this possibility.

METHODS

Methods and any associated references are available in the online version of the paper.

Accession codes. NCBI GEO: microarray data are available under accession number GSE49237.

Note: Any Supplementary Information and Source Data files are available in the online version of the paper.

ACKNOWLEDGMENTS

We thank R. Hevner (University of Washington, Seattle) for the *Tbr1*$^{+/-}$ mice; the Functional and Micro-Magnetic Resonance Imaging Center (supported by the National Research Program for Genomic Medicine, National Science Council, Taiwan, NSC99-3112-B-001-020); S.-Y. Tung, the MicroArray Facility and the Bioinformatics Core of the Institute of Molecular Biology and DNA MicroArray Core Facility of the Institute of Plant and Microbial Biology, Academia Sinica; J. Kung and Animal Facility of Institute of Molecular Biology, Academia Sinica; C.-Y. Chang, W.-R. Wong and C.-W. Tsai for technical assistance; C. Cepko for pCAG-GFP; and M. Loney for English editing. This work was supported by Academia Sinica and the National Science Council of Taiwan (NSC 102-2321-B-001-054 and 102-2321-B-001-029 to Y.-P. H.). T.-N. H. was supported by National Science Council (NSC 102-2811-B-001-060). C.-Y. C. was also supported by National Science Council (NSC 102-2811-B-001-037).

AUTHOR CONTRIBUTIONS

T.-N.H., H.-C.C. and Y.-P.H. contributed to the study design and analyses of data and drafted the manuscript. T.-N.H. performed the ultrasonic vocalization, novel object recognition, histological analyses, DiI tracing, retrograde labeling, local infusion and following behavioral analyses, sequences and microarray analyses. H.-C.C. performed the studies using cultured amygdalar neurons, IUE, quantitative PCR, the rest of behavioral assays and gene expression analyses after behavioral stimulation. S.-J.C. contributed to **Supplementary Figure 2c–e**, technical support on IUE and discussion. W.-H.C. performed the microarray analysis. C.-Y.C. and H.-F.W. confirmed the TBR1 target genes using immunoblotting. T.-N.H. and H.-C.C. contributed equally to this study.

COMPETING FINANCIAL INTERESTS

The authors declare no competing financial interests.

1. Bulfone, A. *et al.* T-brain-1: a homolog of Brachyury whose expression defines molecularly distinct domains within the cerebral cortex. *Neuron* **15**, 63–78 (1995).
2. Remedios, R. *et al.* A stream of cells migrating from the caudal telencephalon reveals a link between the amygdala and neocortex. *Nat. Neurosci.* **10**, 1141–1150 (2007).
3. Hevner, R.F. *et al.* Tbr1 regulates differentiation of the preplate and layer 6. *Neuron* **29**, 353–366 (2001).
4. Yu, T.W. *et al.* Using whole-exome sequencing to identify inherited causes of autism. *Neuron* **77**, 259–273 (2013).
5. Iossifov, I. *et al.* De novo gene disruptions in children on the autistic spectrum. *Neuron* **74**, 285–299 (2012).
6. O'Roak, B.J. *et al.* Sporadic autism exomes reveal a highly interconnected protein network of *de novo* mutations. *Nature* **485**, 246–250 (2012).
7. Neale, B.M. *et al.* Patterns and rates of exonic *de novo* mutations in autism spectrum disorders. *Nature* **485**, 242–245 (2012).
8. Sanders, S.J. *et al.* *De novo* mutations revealed by whole-exome sequencing are strongly associated with autism. *Nature* **485**, 237–241 (2012).
9. O'Roak, B.J. *et al.* Exome sequencing in sporadic autism spectrum disorders identifies severe *de novo* mutations. *Nat. Genet.* **43**, 585–589 (2011).
10. O'Roak, B.J. *et al.* Multiplex targeted sequencing identifies recurrently mutated genes in autism spectrum disorders. *Science* **338**, 1619–1622 (2012).
11. LeDoux, J. The amygdala. *Curr. Biol.* **17**, R868–R874 (2007).
12. Hsueh, Y.P., Wang, T.F., Yang, F.C. & Sheng, M. Nuclear translocation and transcription regulation by the membrane-associated guanylate kinase CASK/LIN-2. *Nature* **404**, 298–302 (2000).
13. Wang, G.S. *et al.* Transcriptional modification by a CASK-interacting nucleosome assembly protein. *Neuron* **42**, 113–128 (2004).
14. Wang, T.F. *et al.* Identification of Tbr-1/CASK complex target genes in neurons. *J. Neurochem.* **91**, 1483–1492 (2004).
15. Huang, T.N. & Hsueh, Y.P. CASK point mutation regulates protein-protein interactions and NR2b promoter activity. *Biochem. Biophys. Res. Commun.* **382**, 219–222 (2009).
16. Furley, A.J. *et al.* The axonal glycoprotein TAG-1 is an immunoglobulin superfamily member with neurite outgrowth-promoting activity. *Cell* **61**, 157–170 (1990).
17. Stoeckli, E.T. & Landmesser, L.T. Axonin-1, Nr-CAM, and Ng-CAM play different roles in the *in vivo* guidance of chick commissural neurons. *Neuron* **14**, 1165–1179 (1995).
18. Kunz, S. *et al.* Neurite fasciculation mediated by complexes of axonin-1 and Ng cell adhesion molecule. *J. Cell Biol.* **143**, 1673–1690 (1998).
19. Nakashiba, T., Nishimura, S., Ikeda, T. & Itohara, S. Complementary expression and neurite outgrowth activity of netrin-G subfamily members. *Mech. Dev.* **111**, 47–60 (2002).
20. Bekirov, I.H., Nagy, V., Svoronos, A., Huntley, G.W. & Benson, D.L. Cadherin-8 and N-cadherin differentially regulate pre- and postsynaptic development of the hippocampal mossy fiber pathway. *Hippocampus* **18**, 349–363 (2008).
21. Muller, C.W. & Herrmann, B.G. Crystallographic structure of the T domain-DNA complex of the Brachyury transcription factor. *Nature* **389**, 884–888 (1997).
22. Won, H. *et al.* Autistic-like social behaviour in Shank2-mutant mice improved by restoring NMDA receptor function. *Nature* **486**, 261–265 (2012).
23. Horio, M., Mori, H. & Hashimoto, K. Is D-cycloserine a prodrug for D-serine in the brain? *Biol. Psychiatry* **73**, e33–e34 (2013).
24. Bauer, E.P., Schafe, G.E. & LeDoux, J.E. NMDA receptors and L-type voltage-gated calcium channels contribute to long-term potentiation and different components of fear memory formation in the lateral amygdala. *J. Neurosci.* **22**, 5239–5249 (2002).
25. Holmes, N.M., Parkes, S.L., Killcross, A.S. & Westbrook, R.F. The basolateral amygdala is critical for learning about neutral stimuli in the presence of danger, and the perirhinal cortex is critical in the absence of danger. *J. Neurosci.* **33**, 13112–13125 (2013).

ONLINE METHODS

Antibodies. The following antibodies were used in this study: TBR1 (TBRC, rabbit)[12,26]; c-FOS (9E6, rabbit)[27], Cell Signaling; CaMKII (ab52476, rabbit)[28] and ER81 (ab36788, rabbit), Abcam; GRIN2B (AB1557P, rabbit)[29], PPP1R1B (AB10518, rabbit), LASP1 (MAB8991, mouse) and acetylcholine transferase (AB144P, goat), GRIN2A (NR2A, 06-313, rabbit)[30], Millipore; MEF2C (10056-1, rabbit), Proteintech; VCP (612183, mouse)[31], BD Transduction Laboratories; GAD67 (G5419, mouse)[32], Sigma; GRIN1 (NR1, 556308, mouse)[33], BD Biosciences Pharmingen; NURR1 (sc-991, rabbit)[34], CUX1 (sc-13042, rabbit) and CDH8 (sc-6461, goat), Santa Cruz Biotechnology; CNTN2/TAG1 (AF-1714, goat)[35], R&D Systems; neurofilament light chain (NB 300-131 rabbit)[36], Novus Biologicals; AMYSIN (IMX-3299, goat), Imgenex; GFP (A6455, rabbit)[37], Invitrogen; SMI-312 (SMI-312R, mouse)[27], Covance. The antibodies with validation profiles in Antibodypedia or 1DegreeBio are underlined.

MRI acquisition and data analysis. Mouse MRI was performed as described[38].

DiI tracing and retrograde bead tracing. Mouse brains perfused with PBS mixed with 2% paraformaldehyde were dissected for DiI tracing. For the inter-amygdalar connection, 2 µl DiI (10 mg/ml) was injected into the basolateral amygdala. To trace the cortical axonal projections, DiI crystal was implanted into the sensory or motor cortex. Brain tissue blocks were then postfixed with 2% paraformaldehyde and stored for either three weeks for the amygdala experiments or eight weeks for the cortex experiments. For retrograde labeling, mice were deeply anesthetized and placed on the Lab Standard Stereotaxic Instrument (Stoelting). After securing the animal to restrict movement, we infused 0.4 µl Red Retrobeads IX (Lumafluor) into the central amygdala (1.45 mm posterior to the bregma, 2.5 mm lateral and 4 mm ventral) or the lateral amygdala (1.06 mm posterior to bregma, 3 mm lateral and 5 mm ventral) for 5 min. Two days later for the central amygdala injection or one week later for the lateral amygdala injection, mice were perfused with PBS and 4% paraformaldehyde after they were killed. Brains were then dissected, post-fixed and sectioned for staining with MEF2C to outline the amygdala. Images were acquired with a confocal microscope (LSM700; Carl Zeiss) equipped with a 63× NA 1.4 oil (Plan-Apochromat; Carl Zeiss) objective lens and Zen 2009 (Carl Zeiss) acquisition and analysis software. The densities of cells with red beads in the lateral amygdala and basal amygdala were determined with ImageJ (NIH).

Immunohistochemistry, immunofluorescence staining, primary amygdalar cultures and morphometry. Brain sections for histology and immunohistochemistry studies were prepared as described previously[39,40]. To examine the expression pattern of c-Fos in brain after behavioral testing, we collected brains 2 h after CTA or fear conditioning training. DAB staining was then performed to visualize the c-FOS expression as described[41]. To outline the amygdala, adjacent brain sections were subjected to acetylcholinesterase stain. The images of adjacent sections stained with c-Fos and acetylcholinesterase were merged with Photoshop (CS3, Adobe). The c-Fos positive cell numbers were then measured with ImageJ (NIH).

For immunofluorescence staining, sections were incubated with anti-c-FOS antibody (1:100), anti-CaMKII antibody (1:250), anti-MEF2C antibody (0.93 µg/ml), or anti-GAD67 antibody (1:250) at 4 °C overnight. After washing and secondary antibody incubation, sections were treated with 4% paraformaldehyde for 10 min to fix the fluorescence signals and then incubated with a second desired primary antibody, followed by staining as described above, except that the different fluorochore conjugated secondary antibody was used. To enhance the TBR1 signal in adult mouse brains, the Tyramide Signal Amplification kit (PerkinElmer Life Sciences) was used as described previously[26], except that the TBR1 antibody, TRBC, was used at a concentration of 0.75 µg/ml.

The method of dissecting the amygdala from P1 mouse pups was as described previously[42]. Calcium phosphate precipitation was used for transfection. To examine the morphology, neurons were incubated with primary anti-GFP (1:250) and anti-SMI-312 (1:500) at 4 °C overnight. Images were acquired using a microscope (AxioImager-Z1; Carl Zeiss) and then quantitatively analyzed with ImageJ (NIH).

DNA microarray. Total RNA isolated from freshly dissected E16.5 mouse forebrains (4 wild-type and 4 *Tbr1*$^{-/-}$) and purified by TRIzol reagent (Invitrogen) was used for cDNA synthesis and further biotin-labeled cRNA hybridization probe generation. RNA quality was first assessed by Agilent Bioanalyzer 2100 with the criteria: the OD260/280 ratio >1.9, the OD260/230 ratio >1.8 and the 28S/18S ribosomal RNA ratio >1.8. RNA hybridization with Affymetrix GeneChip Mouse Genome 430 2.0 Array (Affymetrix) was performed by the DNA Microarray Core Laboratory at the Institute of Plant and Microbial Biology (Academia Sinica, Taipei, Taiwan) according to the manufacturer's instructions. Final image files were detected with an Affymetrix GeneChip Scanner 3000 and the initial DAT files were processed by Affymetrix GeneChip Operating Software (GCOS) to generate the raw signal intensity CEL files. The data were analyzed by GeneSpring GX (version 7.3, Agilent Technologies) with the assistance of the Microarray Core Facility of the Institute of Molecular Biology (Academia Sinica, Taipei, Taiwan). Parameters for normalization were set follows: data transformation, set measurements less than 0.01 to 0.01; per chip, normalize to 50th percentile; per gene, normalize to median and specific samples separately. Transcripts which exhibited statistically significant differences were determined by comparing the *Tbr1*$^{-/-}$ and wild-type conditions with one-way ANOVA analysis, *P*-value cutoff 0.05. The gene-candidate list was further narrowed down by selecting raw probe intensities of higher than 500 in either KO or wild-type combined with a fold-change greater than 1.5-fold in both the up- and down-regulation lists. Multiple testing corrections were also performed with Westfall and Young Permutation (slow). Gene Ontology (GO) analysis (GeneSpring GX) was also applied to determine molecular function, biological process and cellular component clustering.

Quantitative PCR. RNA purification and complementary DNA (cDNA) synthesis were performed with TRIzol (Invitrogen) and the Transcriptor First Strand cDNA Synthesis Kit (Roche), respectively, according to the manufacturers' instructions. Quantitative-PCR of *Tbr1* and *Cntn2* expression were performed using the LightCycler 480 Probes Master kit (Roche) according to the manufacturer's instructions. The *Ntng1* and *Cdh8* expression levels were then analyzed using the SYBR green kit (Roche). The primer sets for *Tbr1* were 5′-CAAGGGAGCATCAAACAACA-3′ and 5′-GTCCTCTGTGCCATCCTCAT-3′. Primer sets for *Cntn2* were 5′-GGGAGCCTGTGCTACAAGAC-3′ and 5′-GCTTTCCAGTAGCGAATCTCA-3′. The primer sets for *Cdh8* were 5′-TGGAATTAATGGATTTTTACCCC-3′ and 5′-TGCCTCATGCAGCCTTACATTT-3′. The primer sets for *Ntng1* were 5′-GAATGCTTCGGCCACTCCAA-3′ and 5′-TCTGAAGTAGCCCAGCCTGCA-3′. The primer sets for *Cyclophilin* (*Cyp*) were 5′-TGCCCAGCAGTTTAGTACCC-3′ and 5′-TGCTTCCCTGTCTCCACAGT-3′.

Plasmid construction. To generate the HA-tagged *Tbr1* mutant (N374H) construct, site-directed mutagenesis was performed with the following oligonucleotide: 5′- GTCACCGCCTACCAGCACACGGATATTACACAACT-3′ (the underlined base indicates the mutated site). To construct the *Cntn2* expression plasmid, the coding sequence (CDS) was amplified by PCR from *Cntn2* IMAGE clone (IMAGE 30362931) and further subcloned into the vector pCAGIG (Addgene #11159). For miRNA knockdown, the oligonucleotides corresponding to *Cdh8* nt 2938-2958 and *Ntng1* nt 2200-2220 were cloned into pcDNA6.2-GW/EmGFP-miR (Invitrogen) to express miR-Cdh8 and -Ntng1, respectively. The plasmid cDNA6.2-GW/EmGFP-miR-neg control predicted not to target any gene in mammalian genomes was used as a negative control for miR-Cdh8 and -Ntng1.

Animals and behavioral assays. The *Tbr1*$^{+/-}$ mice[3] were originally provided by R.F. Hevner (Department of Neurological Surgery, University of Washington, Seattle). These mice were maintained in a facility at Academia Sinica and were backcrossed into a C57BL/6 background for over 15 generations. All of the animal experiments were performed with the approval of the Academia Sinica Institutional Animal Care and Utilization Committee. Wild-type littermates were used as controls. Male animals at 2–4 months of age were used for behavioral assays to avoid variations due to the estrus cycle and age. All of the animals were housed in mixed-genotype groups of 3–5 mice per cages and subjected to experiments randomly without any specific selection. The animals were acclimatized to the test room for at least 1 week before the behavioral assays. A 12-h light/dark cycle (lights off at 20:00) was maintained in the test room. Food and water were accessed *ad libitum*, except during CTA, the T-maze, two-choice digging test and social transmission of food preference experiments. The test order

doi:10.1038/nn.3626

was open field, followed by elevated plus maze, novel object and social behavioral test including reciprocal social interaction, three-chamber social test and social transmission of food preference. Then, the mice were subjected to the cognitive flexibility containing T-maze and two-choice digging test, followed by CTA or auditory fear conditioning. Mice were housed individually for 1 week before the test of reciprocal social interaction and CTA. In the second group of tests, drug-treated mice were subjected to reciprocal social interaction and T-maze followed by amygdala-dependent learning. The above assays were carried out between 10:00 and 18:00 h to prevent fluctuations due to the circadian rhythm.

Open field test and elevated plus maze. The equipment and procedures used in both behavioral tests were as described previously[39,40]. A Smart Video Tracking System (Panlab) was used to determine the time spent in the open arms, the closed arms and the central area during the test.

Auditory fear conditioning. This behavioral paradigm was performed as described[39,40]. The freezing response to total 20 auditory stimulations was measured, and the average percentage freezing in response to the first four tones was taken as the degree of auditory fear conditioning. Freezing responses were videotaped and measured with the FreezeScan 2.0 system (CleverSys).

Appetitively motivated T-maze acquisition and reversal learning. The equipment and procedures were as described previously[39,40]. After mice reached the criterion of acquisition in a T-maze, i.e., 80% correct responses on three consecutive days, they were subjected to reversal learning in which the reward was switched to the opposite arm. In the reversal learning, mice were given 10 trials a day. The number of days taken to achieve an 80% first correct response rate was recorded to indicate flexibility to change.

Reciprocal social interaction and social transmission of food preference. These two behavioral assays were performed as described[39,40].

Three-chamber social behavior test. The apparatus and procedures used in the three-chamber social test were as previously described[39,43]. The time spent interacting or sniffing each wire cage in the left and right chambers was measured using the Smart Video Tracking System (Panlab).

Novel object recognition. The novel object recognition test comprised three parts performed on four days. The first part was habituation. On days 1 and 2, mice were put into a non-transparent box (40 × 40 × 40 cm) for 10 min to allow habituation to the manipulations and environment. On day 3, the first training session was conducted. Mice were put into the same box with two identical objects for 10 min to explore and recognize the objects. On day 4, the final memory test was performed. Mice were individually put into the box with one object from day 3 and one novel object for 10 min. The movements of mice in the box were recorded with a digital camera and analyzed with a Smart Video Tracking System (Panlab).

Conditional taste aversion (CTA). The procedures were as described previously[40]. Briefly, during the 7-day pretraining period, mice were deprived of water in their home cages and put into the experimental cages to receive their daily water for 15 min every day. On the day of training (D0), mice were first offered a sucrose solution (pleasant, new taste; 100 mM, 15 min); then, they were given an intraperitoneal injection of LiCl (malaise-inducing agent; 0.15 M, 20 μl/g of body weight); finally, they were returned to their home cages and observed for diarrhea. As a control, another group of animals received NaCl instead of LiCl injections. Two days after training, mice were presented with a two-bottle test for a 15-min period in the experimental cages. They were offered two drinking bottles; one contained 100 mM sucrose and the other contained water. The sucrose and water intakes were recorded to measure the sucrose preference, where the sucrose preference index = sucrose intake/(sucrose + water intake).

Two-choice digging test. The apparatus and procedures used in this task were as described previously[44–46] with modifications. The test plastic apparatus (25 × 20 × 15 cm) was divided into two identical choice compartments (15 × 10 cm) with an entrance connecting to the waiting compartment (20 × 10 cm). The digging bowl (25 mm in diameter, 45 mm in height) placed in choice compartments was baited with sunflower seeds (30 mg) hidden underneath original- or cinnamon (2%)-flavored sawdust. The procedure consisted of a 3-day habituation period, 1-day learning period and 1-day reversal learning period. Throughout the entire experiment, the mice were food-restricted (1.5–2 g per day). During the habituation phase, mice were given a sawdust-filled baited bowl daily in their home cage to learn to retrieve the reward by digging in the bowl. On the last two days of habituation, the mice were placed into the waiting section, allowed to explore the test box for 10 min daily and immediately given two consecutive trials to freely access two baited bowls (original odor on one day and cinnamon on the other day) placed in choice compartments until both rewards were found. On the day of learning, mice were first trained to learn that the bowl filled with original-flavored sawdust was baited. In the first four trials (training trials), mice were allowed to dig in two bowls, one of which was an original odor sawdust-filled baited bowl (correct) and the other of which was a cinnamon odor sawdust-filled unbaited bowl (incorrect). After training, the mice were allowed to dig in one bowl only. The bowl that the mouse chose to dig in (correct/incorrect) was recorded. If the mouse dug in the correct bowl, it was allowed to consume the reward. The trial was terminated immediately when the mouse started to dig in the incorrect bowl. Once the mouse met a criterion level of six consecutive correct trials, the testing was ended. On the next day, mice were subjected to the reversal learning test in which the reward was switched to the bowl filled with cinnamon-flavored sawdust. Mice were again first given four training trials to relearn that the cinnamon odor sawdust-filled bowl was the correct one and then allowed to immediately choose one bowl only to test their cognitive flexibility. The number of trials needed to reach the criterion (six consecutive correct trials) was recorded on the day of learning and reversal learning period.

Ultrasonic vocalizations of mouse pups. Four-day-old mouse pups were isolated from their home cage and placed in a clean beaker with bedding. Next, the beaker was placed in a soundproof chamber. Ultrasonic vocalizations were recorded for 5 min using the ultrasonic recording model 116H (Avisoft Bioacoustis). The frequency of the vocalizations was then analyzed using Avisoft-SASLab Pro software.

***In utero* electroporation.** The procedures were conducted as described previously[2,47]. The miRNA fragments of pcDNA6.2-GW/EmGFP-miR-Cdh8 and miR-Ntng1 were subcloned into the 3′ untranslated region of the vector pCAG-GFP (Addgene #11150)[48] and purified by Qiagen EndoFree Plasmid Maxi kit. The desired plasmids (1 μg/μl) mixed with 1% Fast Green solution at 1/100 volume were injected into one of the lateral ventricles of an embryo using a fine glass micropipett. The positive electrode (3 mm diameter) was then placed toward the caudal and ventral direction of the telencephalon of the embryo (**Supplementary Fig. 6a**). Five electric pulses (30V, 50 ms pulse length) with 950-ms intervals were performed using BTX electric pulse generator (Electro Square porator ECM 830, Genetronics). Mice were killed at E18.5–19.5 and the GFP fluorescence was then visualized with a confocal microscope (LSM 700; Carl Zeiss) and acquired with Zen acquisition and analysis software (Carl Zeiss).

Pharmacological treatment. For local infusion, two 25 gauge stainless guide tubes were implanted bilaterally into the amygdala (1.7 mm posterior to the bregma, 3.1 mm lateral and 4.7 mm ventral). A 30 gauge dummy cannula was inserted into the guide tube to prevent clogging. Two screws were fixed on the skull and dental cement was used to encase the screws and basal part of guide tube on the skull. After two weeks of recovery, D-cycloserine (10 mg/ml; Ascent Scientific) or ifenprodil (0.5 mg/ml, Sigma) were dissolved in normal saline and injected into the amygdala at a volume of 1 μl and a rate of 0.5 μl/min for 30 min before the behavior tests. For systemic treatment, D-cycloserine was dissolved in saline at a concentration of 12 mg/ml. Thirty minutes before behavioral training, the D-cycloserine was intraperitoneally administered to the wild-type and *Tbr1*$^{+/-}$ mice at a dose of 20 mg/kg. Saline was administered to the mice at a volume of 10 ml/kg, as a vehicle control.

Statistical analysis. Data are presented as means plus s.e.m. Statistical comparisons were performed with unpaired *t*-test (**Fig. 1**, **2b**, **2d–e**, **3c** (Cntn2), 5d-k, 5m, 6c, 6d, 6k-l, 7b-c, 7e-7h S1, S2, S5, S7, S8) and with one-way ANOVA and *post-hoc* Dunnett test (**Fig. 2c**, **5l**) using GraphPad Prism 5.0, or with two-way ANOVA and *post-hoc* Bonferroni test (**Fig. 3a–c**, **5b**,**c**, **6g**, **6h**, **6j**, **6m**, **7d**) using the software SPSS (version 10.0.7C, SPSS Inc., Chicago, Ill, USA). Multiple comparisons were applied for both one-way and two-way ANOVA. Multiple testing corrections with Westfall and Young Permutation (slow) were performed for microarray analysis. The majority of data met the assumption (normal distribution) of these tests, except **Fig. 1j** (BA), 2b (TBR1 and LASP1), 2c (*Tbr1* and *Cdh8*), 3a-3c (primary axonal length), 5e, 5f, 5g, 5l (*Tbr1*$^{+/-}$), 6j, 7b, 7g, S1f (Aq), S5e (BA), S7a (grooming), S7b (closed arm), S8d (PPP1R1B). No statistical methods were used to predetermine sample sizes but our sample sizes are similar to those reported in previous publications[49,50]. Data collection and analysis were

performed randomly but not blind. Only the experiments in **Fig. 5f**,**g**, **7f**,**g** were carried out blind. One of *Tbr1*$^{+/-}$ mice was excluded from **Fig. 5c** because it was so nervous it jumped over the experimental chamber. As an outlier, one wild-type mouse was also excluded from **Supplementary Figure 7a**. An outlier was defined as a value outside the mean ± 3 s.d.

26. Hong, C.J. & Hsueh, Y.P. Cytoplasmic distribution of T-box transcription factor Tbr-1 in adult rodent brain. *J. Chem. Neuroanat.* **33**, 124–130 (2007).
27. Liu, H.-Y. *et al.* TLR7 negatively regulates dendrite outgrowth through the Myd88-c-Fos-IL-6 pathway. *J. Neurosci.* (in the press) (2013).
28. Peter, M. *et al.* Transgenic mouse models enabling photolabeling of individual neurons *in vivo*. *PLoS ONE* **8**, e62132 (2013).
29. Huang, T.N., Chang, H.P. & Hsueh, Y.P. CASK phosphorylation by PKA regulates the protein-protein interactions of CASK and expression of the NMDAR2b gene. *J. Neurochem.* **112**, 1562–1573 (2010).
30. Ruel, J. *et al.* Salicylate enables cochlear arachidonic-acid-sensitive NMDA receptor responses. *J. Neurosci.* **28**, 7313–7323 (2008).
31. Wang, H.F. *et al.* Valosin-containing protein and neurofibromin interact to regulate dendritic spine density. *J. Clin. Invest.* **121**, 4820–4837 (2011).
32. Lin, C.W., Liu, H.Y., Chen, C.Y. & Hsueh, Y.P. Neuronally-expressed Sarm1 regulates expression of inflammatory and antiviral cytokines in brains. *Innate Immun.* **20**, 161–172 (2014).
33. Brose, N. *et al.* Differential assembly of coexpressed glutamate receptor subunits in neurons of rat cerebral cortex. *J. Biol. Chem.* **269**, 16780–16784 (1994).
34. Carloni, M. *et al.* The impact of early life permethrin exposure on development of neurodegeneration in adulthood. *Exp. Gerontol.* **47**, 60–66 (2012).
35. Poliak, S. *et al.* Juxtaparanodal clustering of Shaker-like K+ channels in myelinated axons depends on Caspr2 and TAG-1. *J. Cell Biol.* **162**, 1149–1160 (2003).
36. Yokoyama, K. *et al.* NYAP: a phosphoprotein family that links PI3K to WAVE1 signalling in neurons. *EMBO J.* **30**, 4739–4754 (2011).
37. Chen, C.Y., Lin, C.W., Chang, C.Y., Jiang, S.T. & Hsueh, Y.P. Sarm1, a negative regulator of innate immunity, interacts with syndecan-2 and regulates neuronal morphology. *J. Cell Biol.* **193**, 769–784 (2011).
38. Sun, S.W., Song, S.K., Hong, C.Y., Chu, W.C. & Chang, C. Improving relative anisotropy measurement using directional correlation of diffusion tensors. *Magn. Reson. Med.* **46**, 1088–1092 (2001).
39. Lin, C.-W. & Hsueh, Y.-P. Sarm1, a neuronal inflammatory regulator, controls social interaction, associative memory and cognitive flexibility in mice. *Brain Behav. Immun.* (in the press) (2013).
40. Chung, W.C., Huang, T.N. & Hsueh, Y.P. Targeted deletion of CASK-interacting nucleosome assembly protein causes higher locomotor and exploratory activities. *Neurosignals* **19**, 128–141 (2011).
41. Hsueh, Y.P. *et al.* Direct interaction of CASK/LIN-2 and syndecan heparan sulfate proteoglycan and their overlapping distribution in neuronal synapses. *J. Cell Biol.* **142**, 139–151 (1998).
42. Lesscher, H.M. *et al.* Amygdala protein kinase C epsilon regulates corticotropin-releasing factor and anxiety-like behavior. *Genes Brain Behav.* **7**, 323–333 (2008).
43. Moy, S.S. *et al.* Mouse behavioral tasks relevant to autism: phenotypes of 10 inbred strains. *Behav. Brain Res.* **176**, 4–20 (2007).
44. Colacicco, G., Welzl, H., Lipp, H.P. & Wurbel, H. Attentional set-shifting in mice: modification of a rat paradigm, and evidence for strain-dependent variation. *Behav. Brain Res.* **132**, 95–102 (2002).
45. Birrell, J.M. & Brown, V.J. Medial frontal cortex mediates perceptual attentional set shifting in the rat. *J. Neurosci.* **20**, 4320–4324 (2000).
46. Garner, J.P., Thogerson, C.M., Wurbel, H., Murray, J.D. & Mench, J.A. Animal neuropsychology: validation of the Intra-Dimensional Extra-Dimensional set shifting task for mice. *Behav. Brain Res.* **173**, 53–61 (2006).
47. Tabata, H. & Nakajima, K. Labeling embryonic mouse central nervous system cells by in utero electroporation. *Dev. Growth Differ.* **50**, 507–511 (2008).
48. Matsuda, T. & Cepko, C.L. Electroporation and RNA interference in the rodent retina *in vivo* and *in vitro*. *Proc. Natl. Acad. Sci. USA* **101**, 16–22 (2004).
49. Wang, W.Y. *et al.* Interaction of FUS and HDAC1 regulates DNA damage response and repair in neurons. *Nat. Neurosci.* **16**, 1383–1391 (2013).
50. Sananbenesi, F. *et al.* A hippocampal Cdk5 pathway regulates extinction of contextual fear. *Nat. Neurosci.* **10**, 1012–1019 (2007).

doi:10.1038/nn.3626